2007

FINITE ELEMENT ANALYSIS AND EXPERIMENTAL VERIFICATION OF SOI WAVEGUIDE LOSSES

Harish Srinivasan
University of Kentucky, hsrin2@uky.edu

Abstract of Thesis

FINITE ELEMENT ANALYSIS AND EXPERIMENTAL VERIFICATION OF SOI WAVEGUIDE LOSSES

Bending loss in silicon-on-insulator rib waveguides was calculated using conformal mapping of the curved waveguide to an equivalent straight waveguide. Finite-element analysis with perfectly matched layer boundaries was used to solve the vector wave equation. Transmission loss was experimentally measured as a function of bend radius for several SOI waveguides. Good agreement was found between simulated and measured losses, and this technique was confirmed as a good predictor for loss and for minimum bend radius for efficient design.

KEYWORDS: Waveguides, Bending Loss, Finite Element Analysis, Perfectly Matched Layer (PML), Mode Mismatch Loss

Harish Srinivasan

10/10/2007

FINITE ELEMENT ANALYSIS ANDEXPERIMENTAL VERIFICATION OF SOI WAVEGUIDE LOSSES

By

HARISH SRINIVASAN

DR. TODD HASTINGS

Director of Thesis

DR.YU MING ZHANG

Director of Graduate Studies

10/10/2007

RULES FOR THE USE OF THESIS

Unpublished theses submitted for the Master's degree and deposited in the University of Kentucky Library are as a rule open for inspection, but are to be used only with due regard to the rights of the authors. Bibliographical references may be noted, but quotations or summaries of parts may be published only with the usual scholarly acknowledgements.

Extensive copying or publication of the dissertation in whole or in part also requires the consent of the Dean of the Graduate School of the University of Kentucky.

A library that borrows this project for use by its patrons is expected to secure the signature of each user.

Name	Date

THESIS

HARISH SRINIVASAN

The Graduate School
University of Kentucky
2007

FINITE ELEMENT ANALYSIS AND EXPERIMENTAL VERIFICATION OF SOI WAVEGUIDE LOSSES

THESIS

A thesis submitted in partial fulfillment of the requirements for the degree of Master of Science in the College of Engineering
at the University of Kentucky

By

Harish Srinivasan

Lexington, KY

Director: Dr Todd Hastings, Professor of Electrical Engineering

Lexington, KY

2007

ACKNOWLEDGEMENTS

I would like to thank Dr.Todd Hastings for his immense support and guidance that he has provided me throughout this thesis work. This thesis would not have been possible without his assistance.

I would like to thank Dr. Vijay Singh and Dr. Stephen Gedney for taking the time and being in my committee.

I would like to thank George Spiggle for helping clean the chip and Larry Rice for helping me with the SEM.

I would like to thank my parents for their support throughout my master's program.

CONTENTS

LIST OF FIGURES

LIST OF TABLES

CHAPTER 1: INTRODUCTION

1.1 BACKGROUND

A waveguide is a structure which guides Electromagnetic (EM) waves. The waveguide works on the principle of Total Internal Reflection (TIR). TIR is an optical phenomenon which occurs when a light wave strikes a boundary between two media at an angle greater than the critical angle (measured with respect to the normal to the surface). When light crosses a boundary of two materials with different refractive indices, a portion of the light refracts and propagates in the other medium and another portion reflects into the same medium. When the angle of incidence of the light at the boundary with respect to the normal of the surface increases the refracted portion of the light decreases and at a certain angle, called the critical angle, the light travels along the boundary. If the light meets the boundary at any angle of incidence above this angle, all the incident light reflects back into the same medium as shown in Figure 1. Optical waveguides have many advantages over electrical transmission systems including: greater channel capacity, lower losses, immunity to interference, and secure transmission.

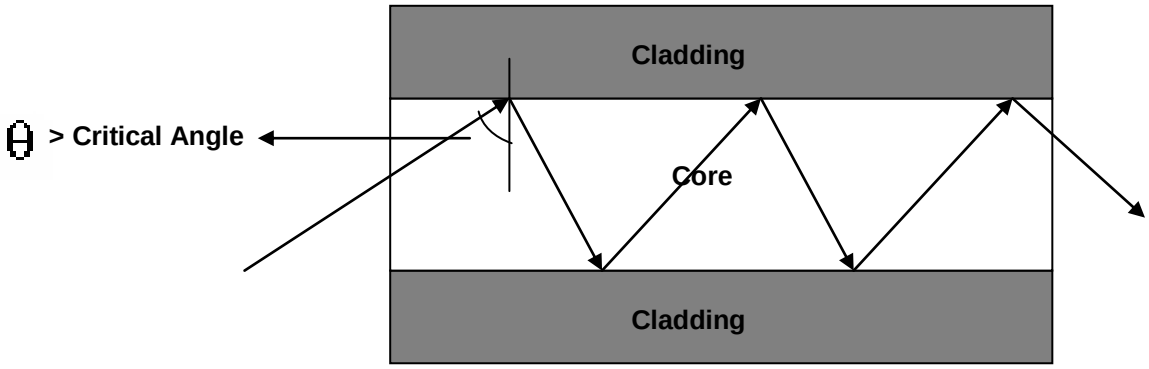

Figure 1: Total Internal Reflection (TIR) in a 1D waveguide. The cladding layers have lower refractive indices than the core.

1.2 SILICON ON INSULATOR WAVEGUIDES

Silicon on insulator (SOI) is a material system consisting of a silicon dioxide layer sandwiched between two layers of silicon. As a result light can be guided in the upper silicon layer, and SOI waveguides have a high refractive index contrast in the vertical direction (Si = 3.48, SiO_2 = 1.44, Air = 1.00 at 1550nm). . The silicon above the oxide layer is etched such that the waveguide has cross sectional dimensions comparable to the optical wavelength to confine light laterally. The cross section of an SOI waveguide is shown in Figure 2.

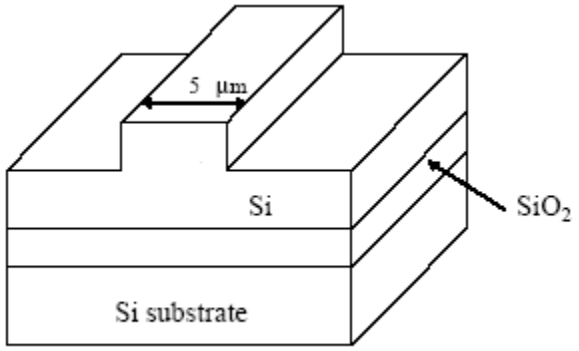

Figure 2 : SOI rib waveguide. Light is confined in the upper silicon layer by the SiO_2 below, air above, and the etched rib structure.

Silicon on insulator (SOI) rib waveguides have proven important for many integrated photonic devices such as wavelength division multiplexing in the telecom industry and as optical interconnects in the electronics industry.[1, 2] In addition, they differ from commonly studied glass, polymer, and III-V semiconductor waveguides by retaining relatively large mode areas despite high index contrast between the core and both the upper and lower cladding layers. Careful simulations of bending loss in these waveguides were recently reported. [3] However, no experimental verification has been carried out to date. Such an analysis, confirmed by experiment, would allow greater confidence in the design of low-loss SOI integrated optics.

To verify that SOI rib waveguide losses can be accurately predicted, we have numerically simulated and experimentally measured loss as a function of bend radius. Calculation of bending loss is typically based on the conformal mapping of a 3D curved

waveguide onto a 1D or 2D equivalent straight waveguide [4-8] or on beam propagation [9] approaches. We chose the former method because of its ease of implementation with a standard 2D solver for the vector wave equation. In such an analysis one must account for the open geometry and here we implement perfectly matched layers (PML) at the simulation boundaries. [10-12]

In this thesis we show that finite element analysis of an equivalent straight waveguide is a good predictor of bending loss and of the minimum bend radius for efficient transmission by comparing the simulation results with the experimental data. It was recently shown that for high index contrast channel waveguides with small bend radii (less than 2 μm) solving the wave equation in cylindrical coordinates system yields more accurate results than the equivalent straight waveguide approximation.[13] However, for waveguides with the substantially larger bend radii considered here (~1cm) we expect both these approaches to give accurate results.

CHAPTER 2: SIMULATION

Finite element analysis was used to simulate the waveguide model for the bending loss and mode mismatch loss. Finite element analysis for the equivalent straight waveguides was carried out using COMSOL Multiphysics v3.2.

A 2D full-vector eigenvalue solver was used to determine the complex propagation constant of the fundamental modes at 1550nm. Each calculated mode was confirmed to be a true guided mode by ensuring the fields were localized at the waveguide rib rather than at the simulation boundary as shown in Figure 3.

In the absence of free charges and currents, the boundary conditions for a guided mode to exist are shown below.

$\mathbf{E_{1\parallel} = E_{2\parallel}}$	Parallel E field is continuous across the boundary
$\boldsymbol{\varepsilon_1 E_{1\perp} = \varepsilon_2 E_{2\perp}}$	Perpendicular component of εE is continuous across the boundary
$\mathbf{B_{1\parallel}} = B_{2\parallel}$	Parallel B field is continuous across the boundary
$\mathbf{B_{1\perp} = B_{2\perp}}$	Perpendicular B field is continuous across the boundary

The wave equation is used to solve for the field and is given by:

$$\nabla \times (\varepsilon_r^{-1} \nabla \times H) - k_0^2 \mu_r H = 0$$

COMSOL discretizes the waveguide into elements and then solves for the electric or magnetic field across each element numerically. The above boundary conditions are applied between elements with different properties. The solver is then used to solve for the complex propagation constant of the model.

.

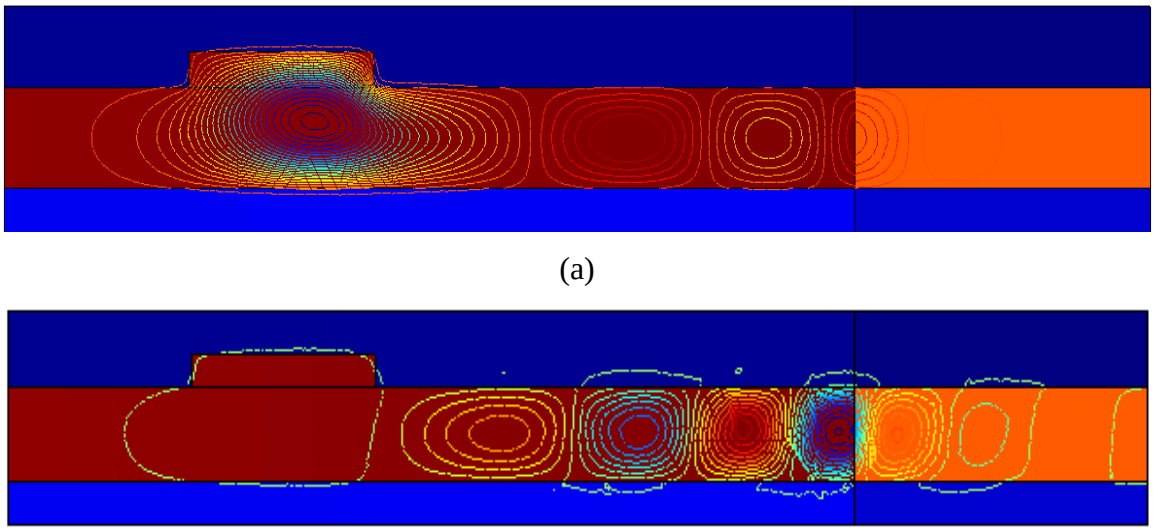

(a)

(b)

Figure 3 : Mode profile of (a) guided mode (b) spurious mode

2.1 WAVEGUIDE GEOMETRY

The top view of the waveguide is shown in Figure 4. The waveguide geometry of interest consists of a 5μm wide rib extending 750nm above a 2.25μm thick silicon slab as shown in Figure 5. A 2μm thick SiO_2 layer provides the lower cladding and air was used as the upper cladding. Due to slight over etching the 750nm rib height places the waveguide design on the edge of single mode operation. Finite element simulations indicate that the waveguide supports a very weakly guided second order mode with the electric field at -3dB expanding to approximately 10μm from the waveguide center for the TE mode as shown in Figure 6. This mode is not strongly excited and becomes extremely lossy in the curved waveguide segments; therefore, it is not surprising that our experimental measurements showed little evidence of multimode behavior.

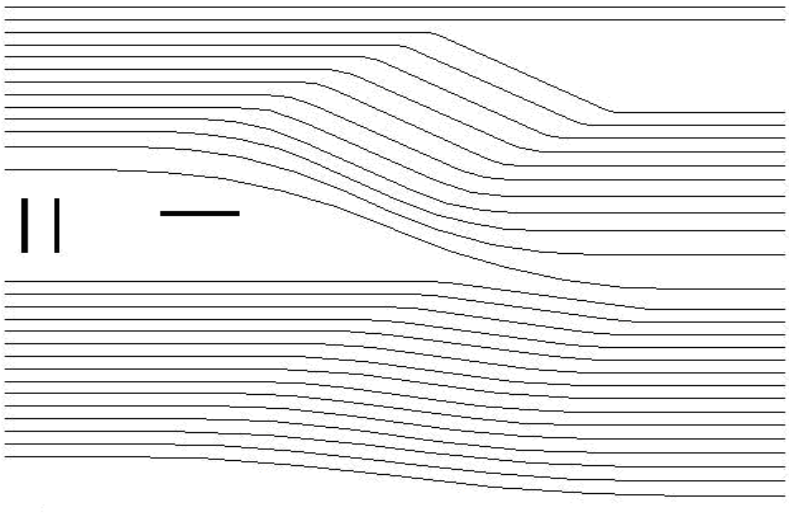

Figure 4 : Waveguide top view

Each of the waveguides had two identical curved sections of varying radii from 0.29 cm to 1.8 cm and a 10 degree rotation. The total length (straight and the bent portions) of the waveguides was 1.1046cm. The constant waveguide length allows bending loss to be distinguished from coupling, absorption, and scattering losses. In addition, the lateral offset between input and output waveguides minimizes the collection of unguided light in the sample.

All the waveguides on which the measurements were acquired had dimensions which fell on the boundary which demarcates single mode and multi mode waveguides. This means that these waveguides do support more than one mode, but the dimensions of the waveguides are such that the higher order modes are very lossy and do not influence the loss data very much.

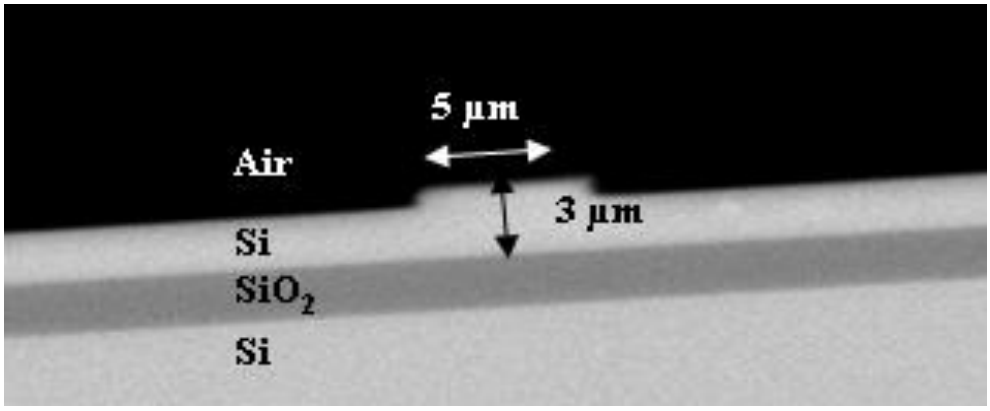

Figure 5 : Scanning Electron Microscopy image of SOI waveguide with materials and dimensions labeled.

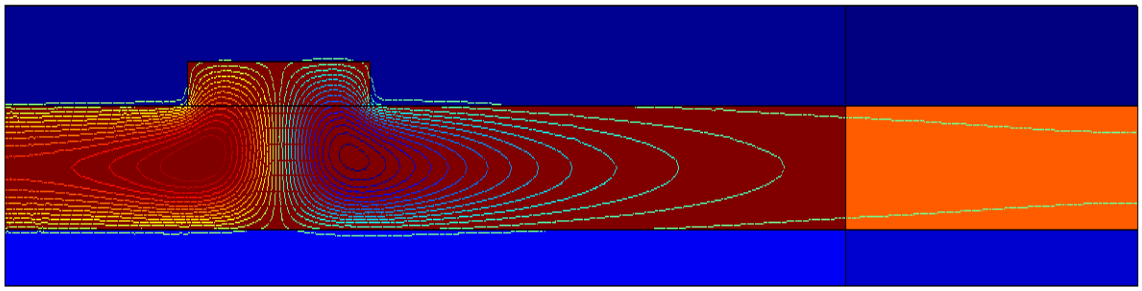

Figure 6 : FEM solution of the second order mode.

2.2 BEND LOSS

Bend loss occurs when the light propagates through the bent portion of the waveguide. When the light propagates through the bent portion of the waveguide, some of the light is lost due to radiation this occurs through out the entire bent portion of the waveguide. The mode in the bent waveguide and the straight waveguide do not look alike. The mode in the bent portion shifts to the outer edge of the waveguide bend and hence the mode looks different. The guided mode in the straight waveguide does not satisfy the boundary condition at the bent portion and hence the mode changes to satisfy the boundary condition.

The mode in the bent portion of the wave has a guided part and a leaky part. The absorption of these leaky waves in the PML regions gives the bending loss in the waveguide. The propagation constant of a mode in a waveguide, denoted by β, determines how the phase and amplitude of light with a given frequency vary along the direction of propagation. To estimate bending loss the 3D curved waveguide was conformally mapped onto a 2D waveguide. Figure 7 shows the electric field distributions in both straight and curved waveguides. The bending loss is given by:

$$\text{bend loss (dB)} = 10 \cdot \log\left(\exp\left(-2\beta_i \cdot l\right)\right)$$

where β_i is the imaginary part of the propagation constant and l is the length of the bend. The imaginary part represents the optical gain if negative or optical loss if positive.

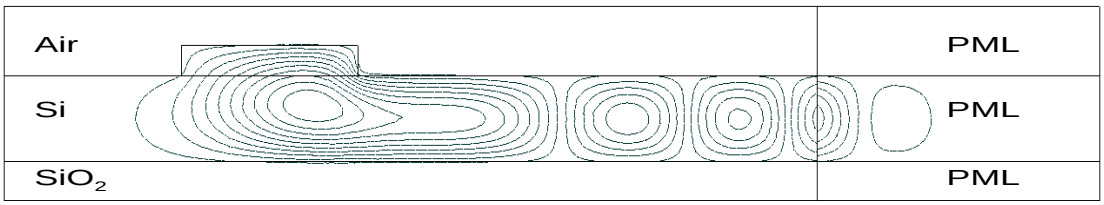

(a)

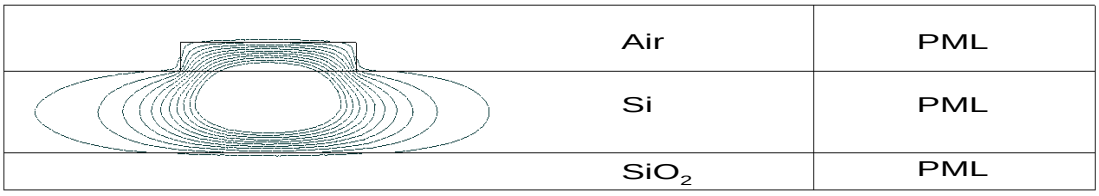

(b)

Figure 7 : TE mode electric field distribution for (a) bent waveguide with bend radius of 0.28851 cm and (b) straight waveguide. Contours represent the x-component of the electric field and are spaced by 10% of the maximum field

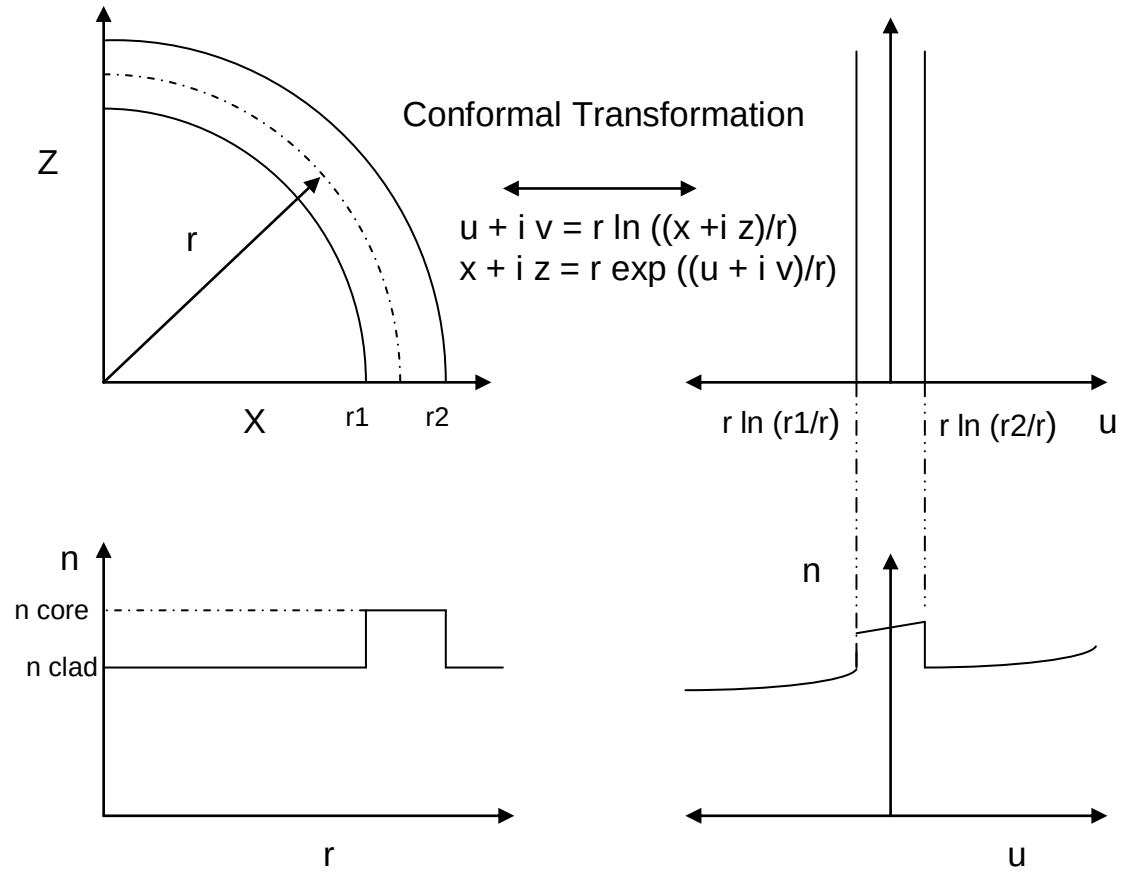

Figure 8 : Conformal mapping of a bent waveguide onto a straight waveguide. Picture adapted from [14] (page 113 Fig 6.7)

Conformal transformation reduces a three dimensional problem to a two dimensional problem with an equivalent index profile as shown in Figure 8. Conformal transformation finds the solution in terms of new variables (u and v) which are related to the Cartesian coordinates x and z by conformal mapping. The variable u represents variations in the radial direction and v represents variations in the angular direction. The new index profile varies continuously except at the waveguide boundaries. The refractive index varies exponentially as opposed to having a piecewise constant is due to the fact that the light in the outer cladding has to travel a greater distance than the light in the core and that the velocity of light in the core and the cladding are different. The exponentially increasing refractive index compensates for the larger distance the light travels with a larger refractive index.

2.3 PML DESIGN

There are several ways to solve open boundary simulation problems using numerical techniques with radiation boundary conditions, absorbing boundary condition, etc. These methods have their own limitations wherein the waves are fully absorbed only if they are plane waves and the direction of propagation is perpendicular to the boundary. Perfectly Matched Layers solve this issue by absorbing the outgoing wave at any angle of incidence and wavelength.

Perfectly Matched Layer's (PML) are non physical regions which are used to numerically solve unbounded free space simulation problems.[12] PML's create a non physical domain around the physical domain which produce no reflection and at the same time attenuate the propagating wave in the PML region. PML regions are modeled using anisotropic complex dielectric constants to both eliminate reflections and to absorb radiated light from the curved waveguide. [10] As a result, the imaginary part of the calculated propagation constant represents bending loss. In this case, the dielectric constants of the perfectly-matched layers were selected to match the dielectric constant at the edge of each equivalent straight waveguide region. Simulations were run to determine the value of the absorption constant and the width of the PML regions that made sure the wave propagated several mesh elements before being completely absorbed. The values of the parameters of the perfectly matched layers are specific to a design and should be appropriately chosen. A model of the waveguide with the PML is shown in Figure 9.

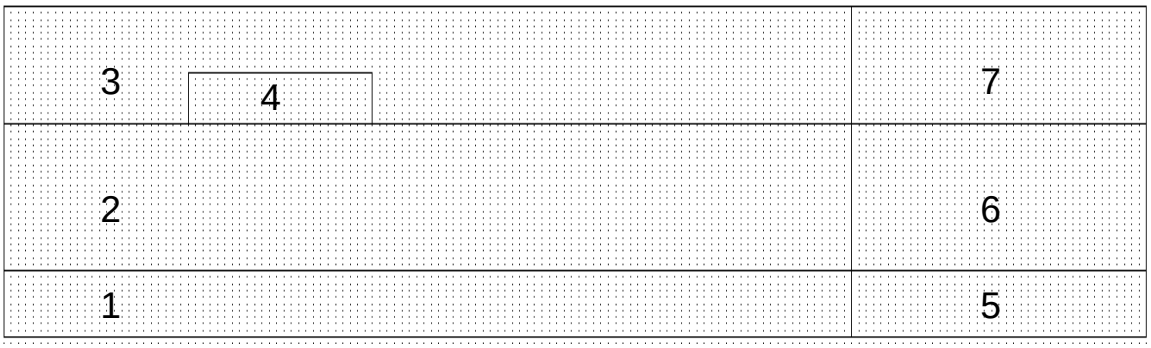

Figure 9 : Sub domain mode of the FEM Model of the waveguide. The regions represent (1) SiO_2 (2) Si, (3) Air, (4) Si, (5,6,7) PMLs.

The equation for permittivity in the different sub-domains in shown below. The permittivity equation is based on the linear approximation of the curved waveguide.

ε (sub-domain 1) = 1.455^2*(1+2*(x-C)/R)

ε (sub-domain 2) = 3.5^2*(1+2*(x-C)/R)

ε (sub-domain 3) = 1*(1+2*(x-C)/R)

ε (sub-domain 4) = 3.5^2*(1+2*(x-C)/R)

$$\varepsilon \text{ (sub-domain 5)} = \begin{bmatrix} 1.455^2*(1+2*(23e\text{-}6\text{-}C)/R)*Lxx & 0 & 0 \\ 0 & 1.455^2*(1+2*(23e\text{-}6\text{-}C)/R)*Lyy & 0 \\ 0 & 0 & 1.455^2*(1+2*(23e\text{-}6\text{-}C)/R)*Lzz \end{bmatrix}$$

$$\varepsilon \text{ (sub-domain 6)} = \begin{bmatrix} 3.5^2*(1+2*(23e\text{-}6\text{-}C)/R)*Lxx & 0 & 0 \\ 0 & 3.5^2*(1+2*(23e\text{-}6\text{-}C)/R)*Lyy & 0 \\ 0 & 0 & 3.5^2*(1+2*(23e\text{-}6\text{-}C)/R)*Lzz \end{bmatrix}$$

$$\varepsilon \text{ (sub-domain7)} = \begin{bmatrix} 1*(1+2*(23e\text{-}6\text{-}C)/R)*Lxx & 0 & 0 \\ 0 & 1*(1+2*(23e\text{-}6\text{-}C)/R)*Lyy & 0 \\ 0 & 0 & 1*(1+2*(23e\text{-}6\text{-}C)/R)*Lzz \end{bmatrix}$$

Where L is a diagonal tensor with the following properties:

$$Lxx = Sy*Sz/Sx$$

$$Lyy = Sz*Sx/Sy$$

$$Lzz = Sx*Sy/Sz$$

and

$$Sx = 1 - j*b$$

$$Sy = 1$$

$$Sz = 1$$

Where Sx, Sy, and Sz are complex valued coordinate scaling parameters and b represents absorption coefficient.

2.3.1 PML DISTANCE FROM THE WAVEGUIDE

Choosing the starting coordinates of the PML from the waveguide is important to obtain an accurate value of the bending loss. The starting coordinates of the PML were not chosen close to the waveguide so as to eliminate the possibility of the PML absorbing the guided wave. Figure 10 (a) shows a simulation where the PML absorbs the guided portion of the wave and this will lead to an incorrect value of the bending loss. The PML was placed in such a way that the leaky modes propagated a few cycles before reaching the PML boundary. This was done to ensure that the PML absorbed the radiated wave and not the guided wave. Figure 10 (b) shows how the leaky modes propagate a few cycles before it reaches the PML boundary and the PML absorbs the leaky modes and not the guided mode.

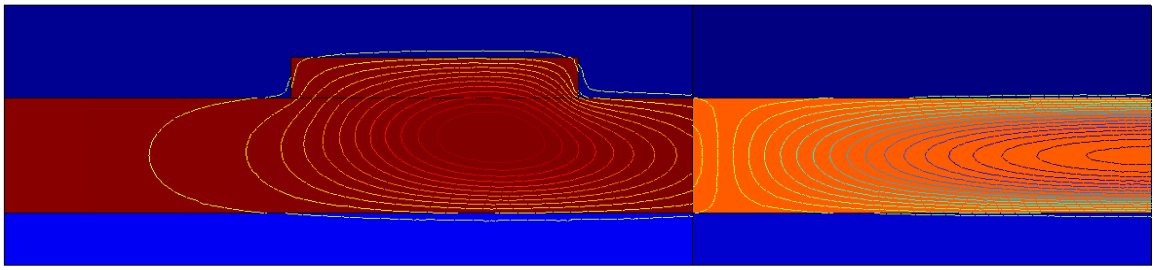

(a)

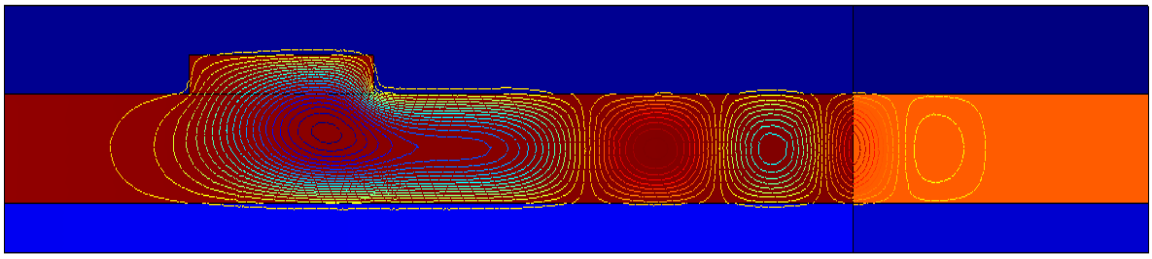

(b)

Figure 10 : PML Design (a) Incorrect design (b) Correct design

Figure 11 shows how the bending loss varies as a function of the PML distance from the waveguide. When the PML is closer to the waveguide and it absorbs the guided wave and the power loss is higher. When the PML is moved further away from the waveguide, it absorbs only the leaky wave and the power loss does not vary much with distance. The loss oscillation that is seen in the graph is due to the reflections from the boundary of the PML. The PML was chosen as near to the waveguide as possible to reduce the simulation run time and that the reflection interfered destructively to calculate the worst case bending loss.

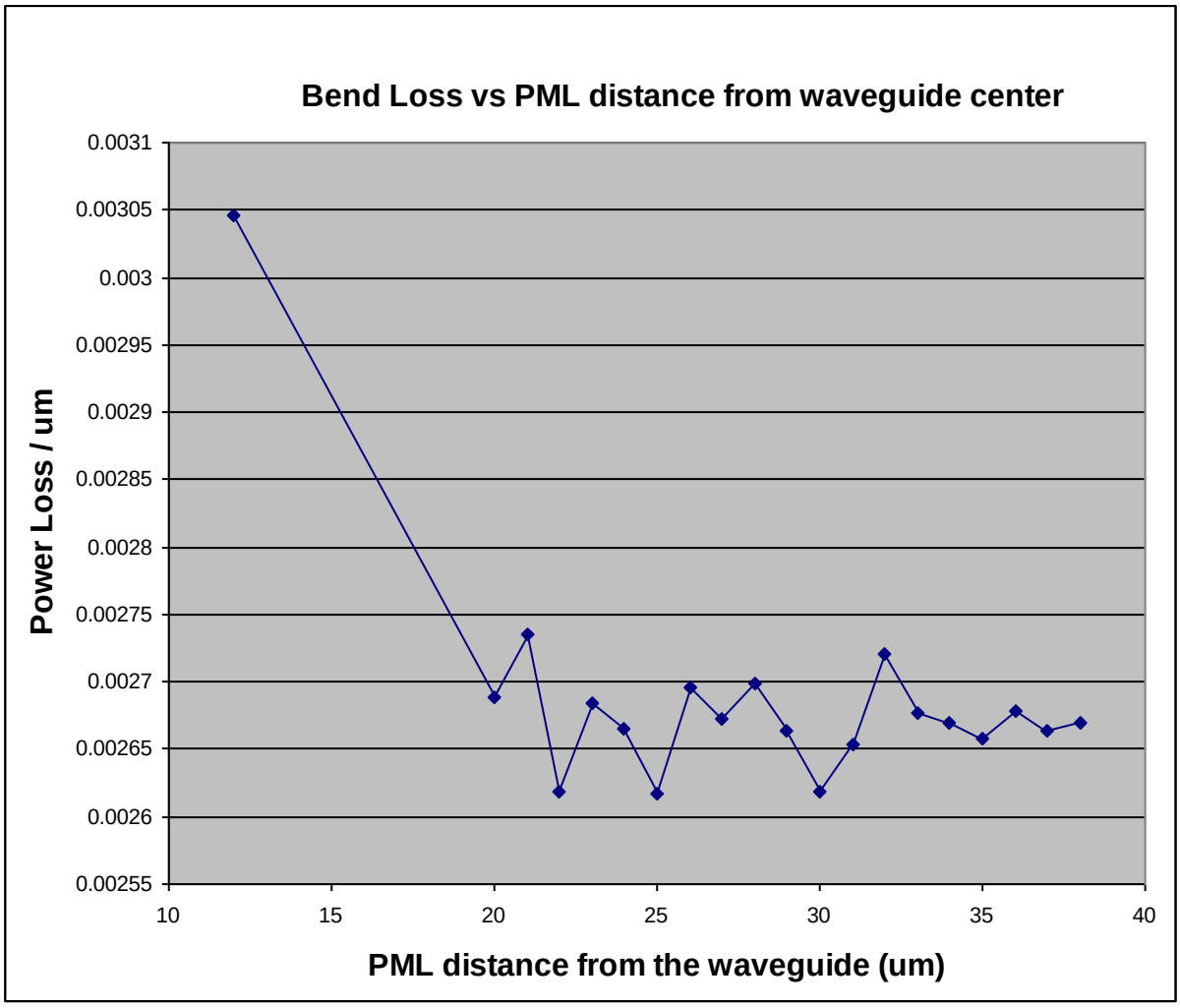

Figure 11 : Bending Loss variation with PML distance form the waveguide

2.3.2 DETERMINATION OF ABSORPTION CONSTANT

We can define perfectly matched layers (PML) in Comsol Multiphysics with materials having anisotropic permittivity and permeability which matches the permittivity and permeability of the physical medium inside the layer in such a way that there are no reflections.

The absorption coefficient was chosen such that the mode penetrates several elements into the PML before the wave is completely absorbed. This is important because if the chosen absorption coefficient is too high the wave is completely absorbed within the first few PML elements leading to significant errors in the propagation constant. If the absorption coefficient is too low then the wave would propagate the entire length of PML and would not be absorbed and would then yield an inaccurate bending loss. Figure 12 shows how the mode of the bent waveguide changes with absorption coefficient. The bend loss is a function of the absorption constant as shown in Figure 13. The loss would initially be zero for an absorption coefficient of zero as there would be no absorption and the wave would propagate without any attenuation. As the absorption coefficient increases, the loss is essentially constant, but increases slightly as less of the wave penetrates to the edge of the PML region. When the absorption coefficient becomes very large the entire wave is absorbed within the first few elements at the boundary of the physical domain and the PML region. This leads to a significant increase in the absorption. The appropriate value of the absorption coefficient would be one which allows the wave to propagate an optimum distance before getting completely absorbed inside the PML region.

The effect of the reflections from the boundary of the physical domain and PML was taken into consideration while deciding on the length of the PML. Simulations were run and the reflections from the boundary were studied. The PML length was so chosen such that the loss due to reflections was maximum (the reflected wave interfered destructively).

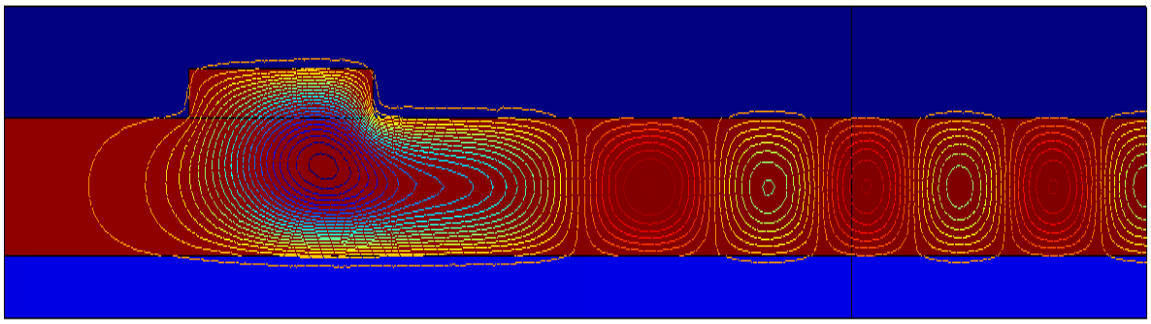

(a)

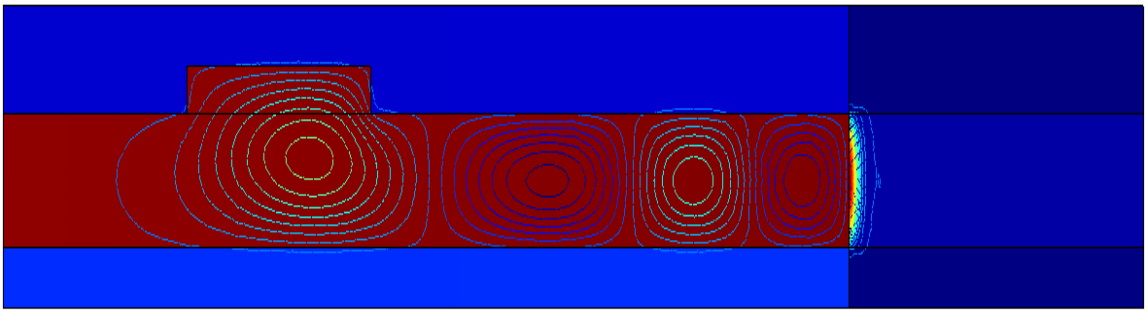

(b)

Figure 12 : Effect of absorption coefficient on the field distribution (a) low absorption coefficient (b) high absorption coefficient

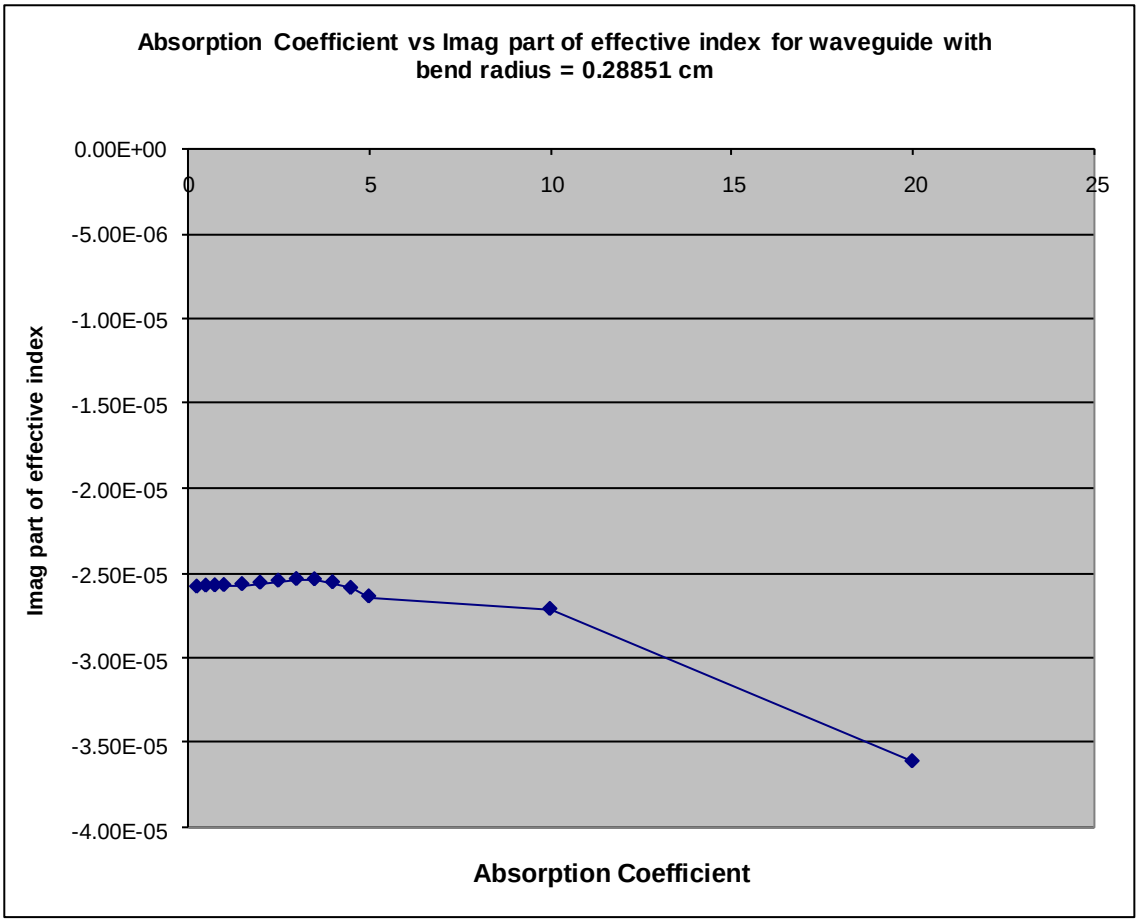

Figure 13 : Effect of PML absorption coefficient on calculated bend loss. The imaginary part of the mode effective index (shown) correlates directly with bend loss.

2.4 MODE MISMATCH LOSS

The particular electromagnetic field distribution of the light in an optical fiber or a waveguide is known as a mode. Depending on the cross section, refractive index and the wavelength a waveguide can support more than one mode. When light is propagating in the waveguide in a particular mode and if it encounters a bend, the light wave propagates in the direction of the bend but with a different electromagnetic field distribution. It is well established that the mode of the straight waveguide is not exactly matched to the mode of the bent waveguide and that this mismatch introduces additional loss. Mode mismatch loss is the radiation loss that occurs at every junction of the straight and bent waveguide and can be calculated from the overlap integral of the electric field in between the two modes. Figure 14 shows the modes of the straight and bent waveguide and the non overlapping part of the fields in the straight and bent waveguide give the power loss.

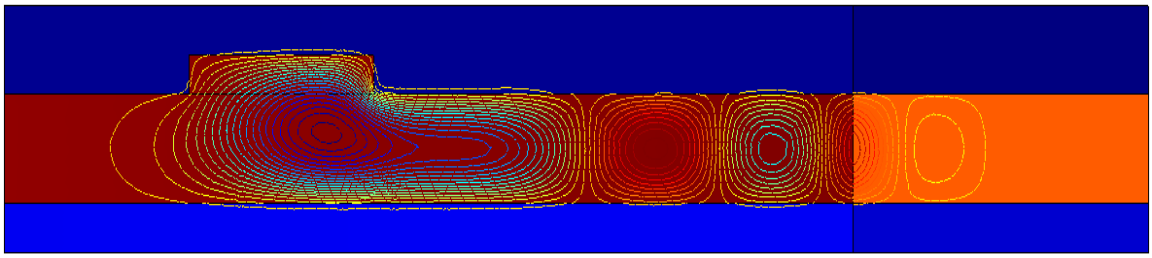

(a)

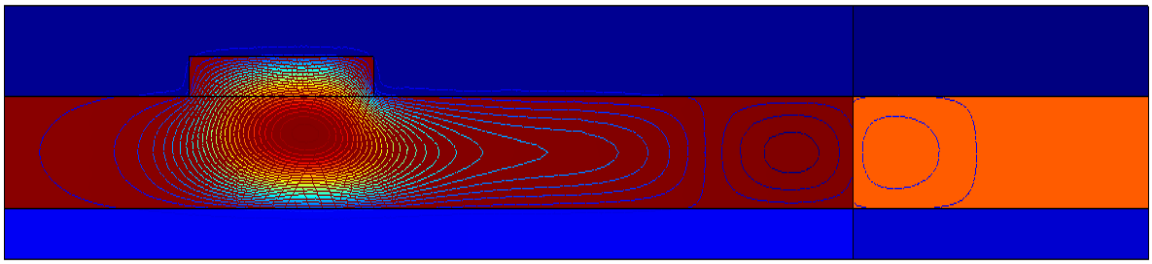

(b)

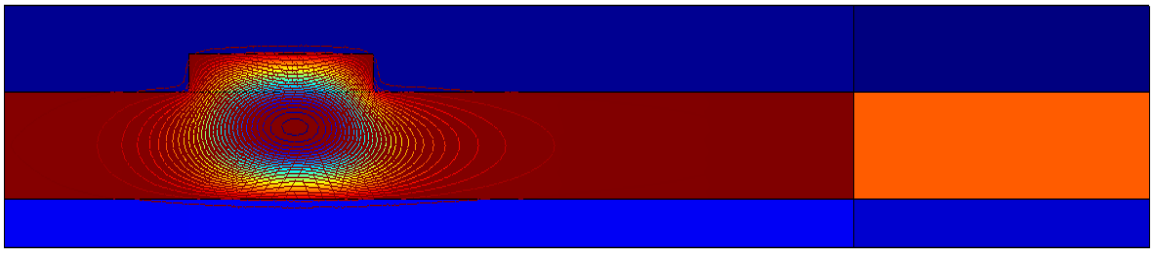

(c)

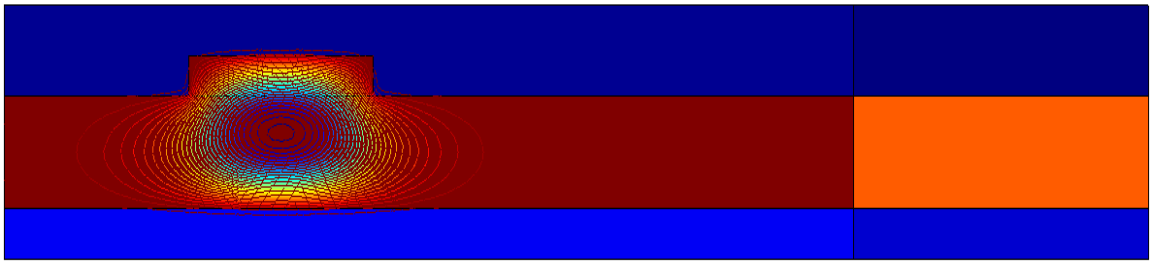

(d)

Figure 14 : FEM simulated field distribution of the straight and bent waveguide (a) r=0.28851 cm (b) 0.49988 cm (c) 0.72111 cm (d) straight waveguide

Mode mismatch loss =

$$\frac{\left|\int\int (E_{sx}\ E_{bx}^{*} + E_{sy}\ E_{by}^{*})\ dA\right|^2}{\int\int (E_{sx}\ .\ E_{sx}^{*} + E_{sy}\ E_{sy}^{*})\ dA\ .\ \int\int (E_{bx}\ .\ E_{bx}^{*} + E_{by}\ E_{by}^{*})\ dA}$$

where E_{sx} and E_{sy} are the electric field components in the x and z directions of the straight waveguide and E_{bx} and E_{by} are the electric field in the x and z directions of the bent waveguide. The area of integration includes the non-radiative portion of the electric field profile.

MATLAB code was written to calculate the mode mismatch loss based on the simulated field profiles. The finite element results for the fields were projected on a uniform grid for the purposes of these calculations. As there were four junctions between straight and bent waveguides, the total mode mismatch loss included in the simulation result is four times the calculated value for a single junction.

2.5 COUPLING LOSS

Coupling loss is another mode mismatch loss which occurs when the light from the optical fiber or lens is coupled to the waveguide. Here too, the electromagnetic field distribution or the mode of the optical fiber or the lens differs from the mode of the waveguide. A commonly used method to couple the light from the optical fiber to the waveguide is known as fiber coupling where the facets of the waveguides are polished and the light from the fiber is focused directly onto the waveguide as shown in Figure 15.

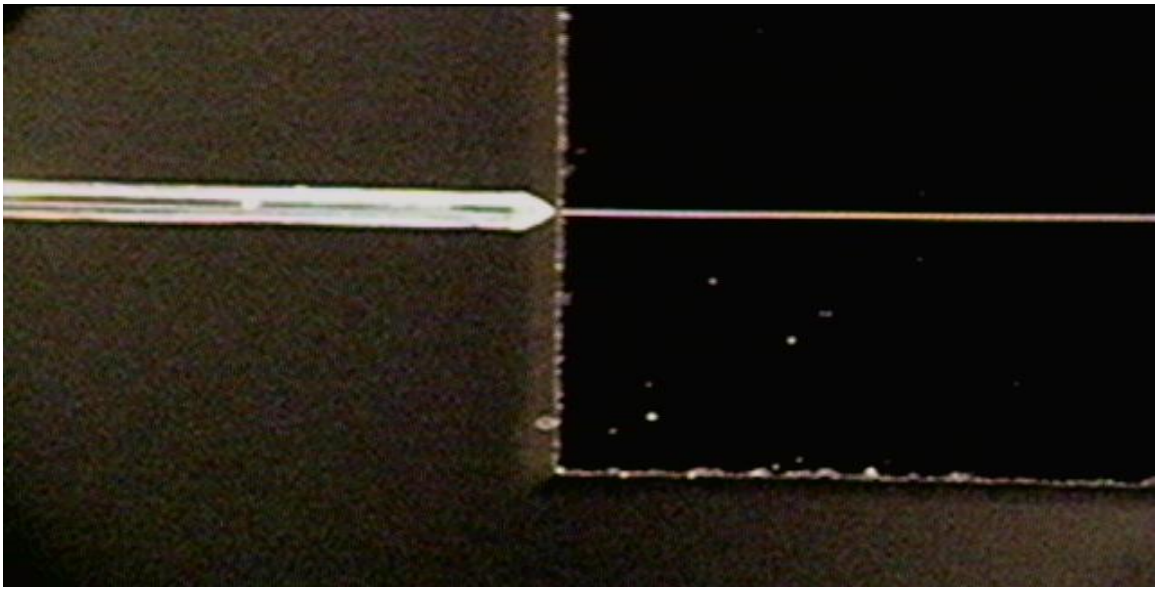

Figure 15 : Lensed optical fiber aligned to a SOI waveguide.

Another solution is to use lenses to couple the light onto the waveguide as shown in Figure 16. The lens focuses the light into an approximately Gaussian spot that better matches the waveguide mode and results in less loss.

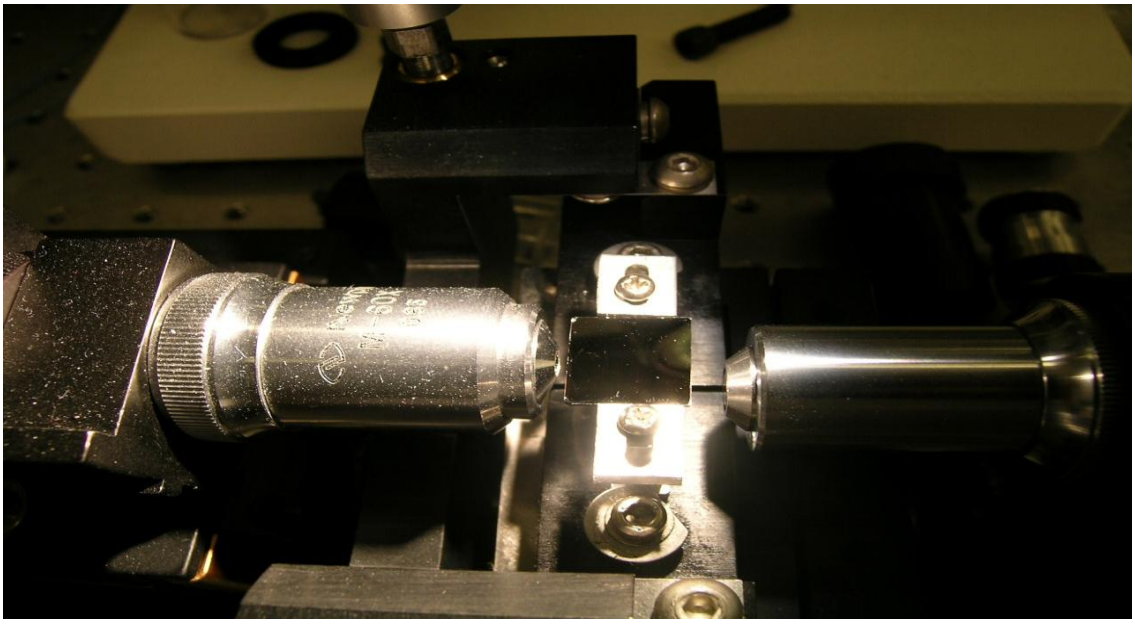

Figure 16 : Lenses aligned to the input and output facets of a SOI waveguide.

The coupling loss is also calculated using the overlap integral of the field distribution between the beam waist produced by the lens and the mode in the waveguide. The field distribution of the wave in the lens is given by the formula:

$$E_s = E_o \exp(-r^2/w_0^2)$$

Where E_0 is the maximum field and is found by normalizing the power in the z- direction to 1. E_0 is found by the following equation:

$$\int_{-\infty}^{\infty}\int_{-\infty}^{\infty} [E_0 \exp(-(x^2+y^2)/\omega_0^2)]^2 \, dx\, dy = 1$$

Where ω_0 is the Gaussian beam radius at which the intensity has reached to $1/e^2$ of its peak value.

The minimum beam waist is calculated using the formula:

$$\omega_0 = (2 \lambda F / D \pi)$$

where D is the diameter of the input collimated beam, F is the focal length and λ is the wavelength

While calculating the overlap integral, the field maximum of the mode in the lens and the waveguide must coincide and hence the origin of the mode in the waveguide should be chosen in such a way that the overlap integral is maximum. Figure 17 shows the point where the electric field is maximum. As seen from the electric field distribution the field is not maximum at the center and simulations were run to find the point of field maximum before the overlap integral is calculated.

There are also reflections from the surface of the waveguide when light is coupled onto the waveguide. For our calculations this reflection is assumed to be a constant which is 30% (reflection at an air to silicon interface). However, additional loss could result from scattering if the waveguide facet is not perfectly smooth.

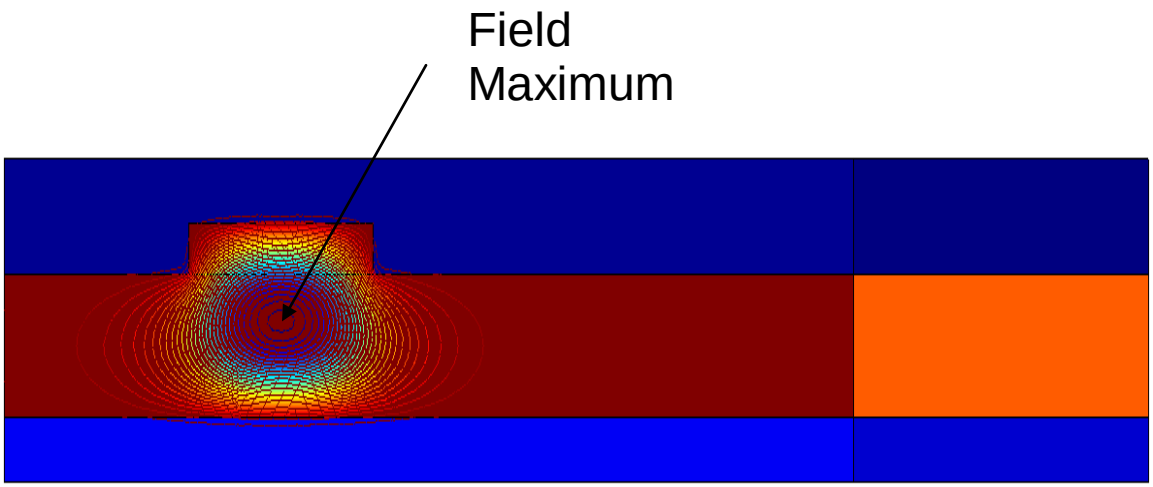

Figure 17 : Point of field maximum for the straight waveguide.

Table 1 : Coupling Loss between the Input Lens and the waveguide due to mode mismatch.

	TE Mode	TM Mode
Input Coupling Loss (db)	-2.0627	-1.9916

As the output lens collects all the light from the waveguide the coupling loss at the output side is zero. Table 1 shows the input coupling loss.

2.6 SCATTERING LOSS

Scattering loss arises from roughness at the sidewalls of the waveguide when light get reflected. The presence of roughness couples the otherwise lossless guided modes to radiated waves. Scattering loss can be modeled if one knows the power spectrum, i.e. amplitude as a function of spatial frequency, of the roughness and the overlap of the electric field with the rough interface.[15] In the absence of specific knowledge of the power spectrum, one can determine the functional dependence, though not the exact value, of bending loss based solely on overlap integral. The goal of this section is to determine whether scattering loss is a function of bend radius and whether scattering loss will influence the measured relationship between losses and bend radius.

Figure 18 shows the mode of a bent waveguide and the arrows indicate the boundary where the maximum scattering is likely to occur. These interfaces are lithographically defined and plasma etched and as a result shows significantly more roughness than the horizontal interfaces defined by epitaxial crystal growth.

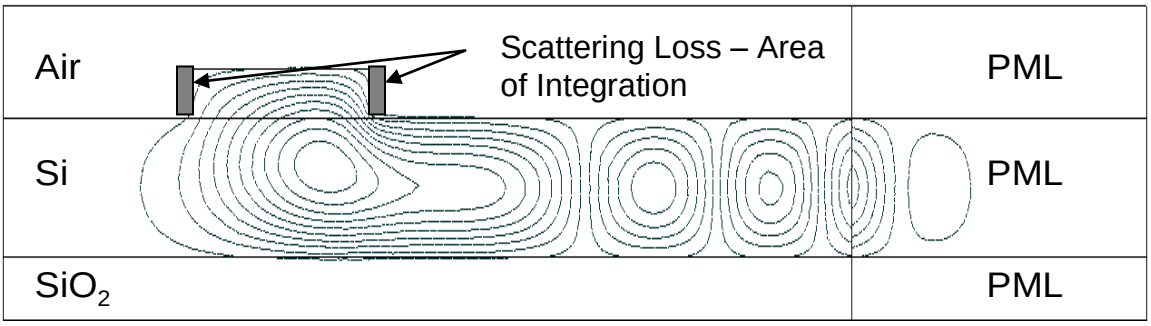

Figure 18 : Scattering loss occurs mostly at the sidewalls as indicated by the arrows

Scattering loss is calculated by the mode overlap integral of the field in the straight waveguide and the field in the bent waveguide at the side walls of the waveguide the area of integration is shown in the figure above. The integration area was 1 μm starting from the waveguide sidewall and extending in the air region. This integration was done at both the sidewalls.

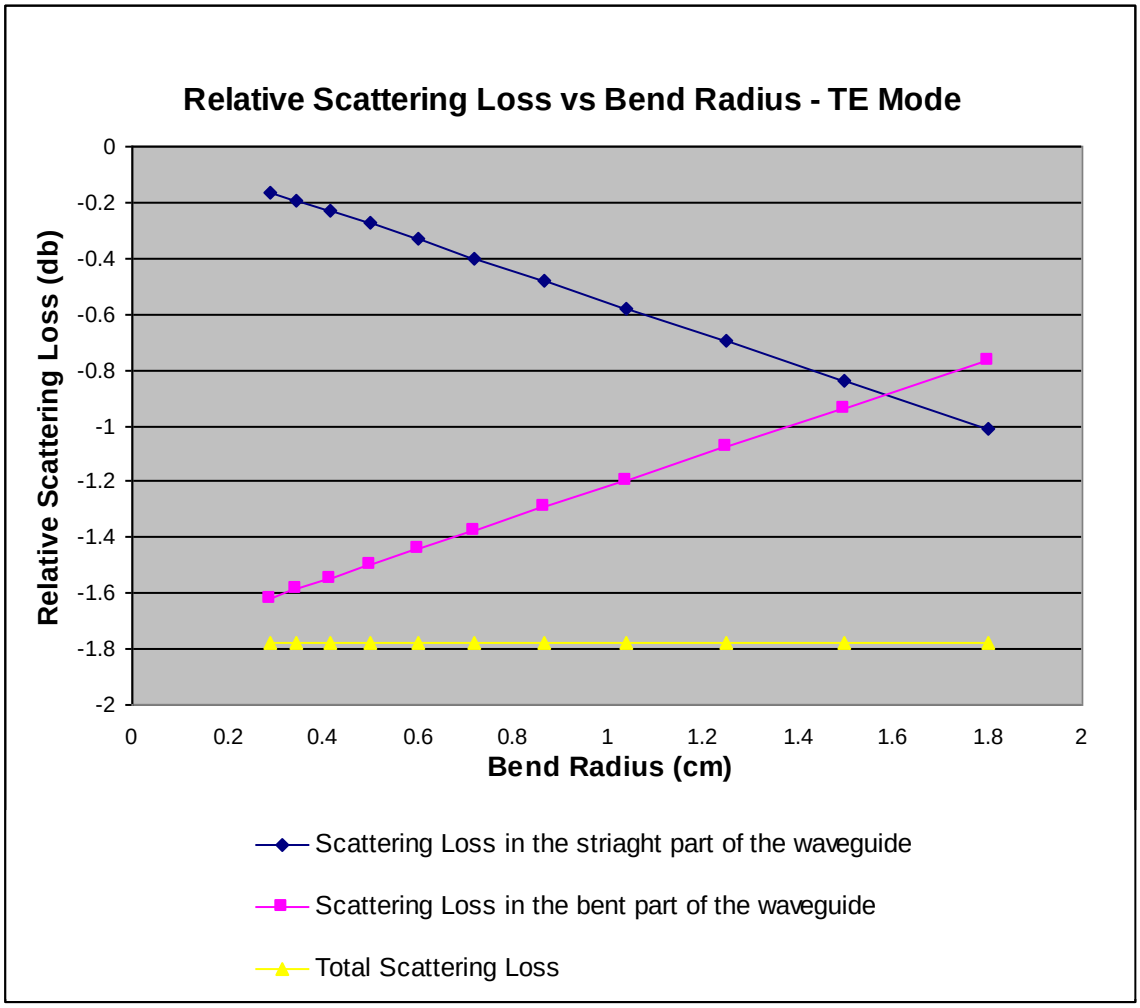

Figure 19 : Variation of scattering loss with bend radius for the TE mode of the SOI waveguide. Values indicate the relative power confined in the rough region at the edge of the waveguide.

Figure 19 shows the variation of scattering loss as a function of bend radius. Scattering loss simulated includes the loss occurring at the sidewalls of the bend and the straight portion of the waveguide chip. In the tightly bend waveguides the scattering loss at the bends are greater when compared to the waveguides with high bend radius. But, the straight portion is longer for the waveguides with large bend radius and hence the total scattering loss of the measures waveguides for all bend radii is approximately the same as seen in the graph.

2.7 FABRY PEROT INTERFERENCE

Another source of measured loss that is possible in experiments is due to reflections at the lens surface and the surface of the silicon chip. The reflection occurs if the lens or the silicon surfaces are very well polished. The reflections can interfere with the forward propagating wave either constructively or destructively. This interference is call Fabry-Perot interference. A plot of transmission loss vs. wavelength reveals Fabry-Perot interference and is shown in Figure 20 for the TE and the TM modes with and with out the waveguide chip in place. It can be seen that the period of oscillations is the same but the magnitude varies over a range of approximately 3db.

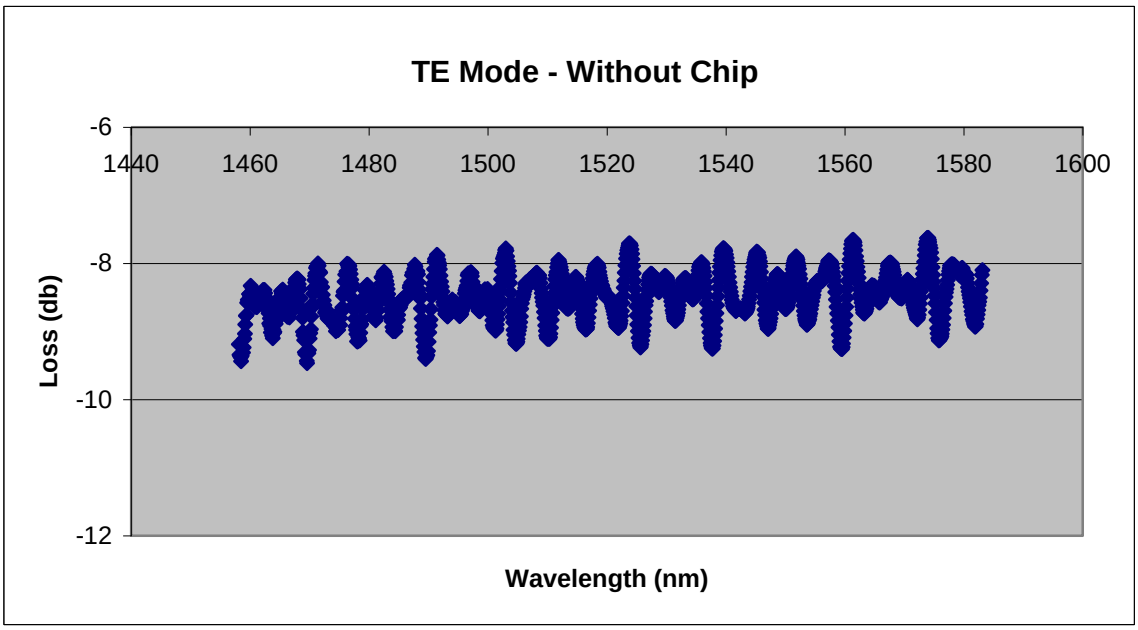

(a)

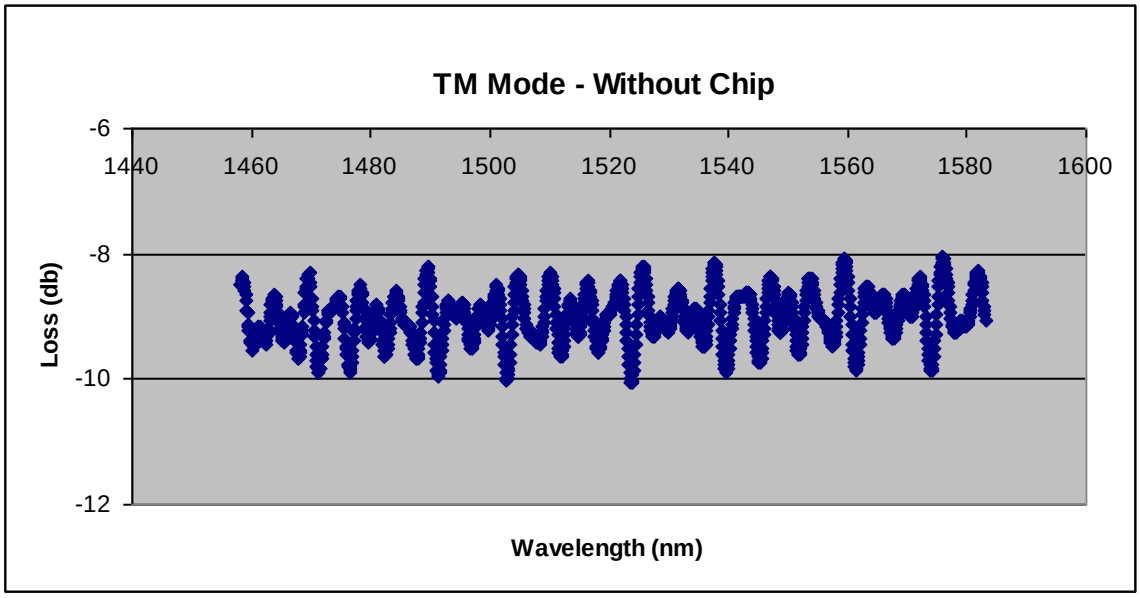
TM Mode - Without Chip
-6
-8
-10
-12
Loss (db)
1440
1460
1480
1500
1520
1540
1560
1580
1600
Wavelength (nm)

(b)

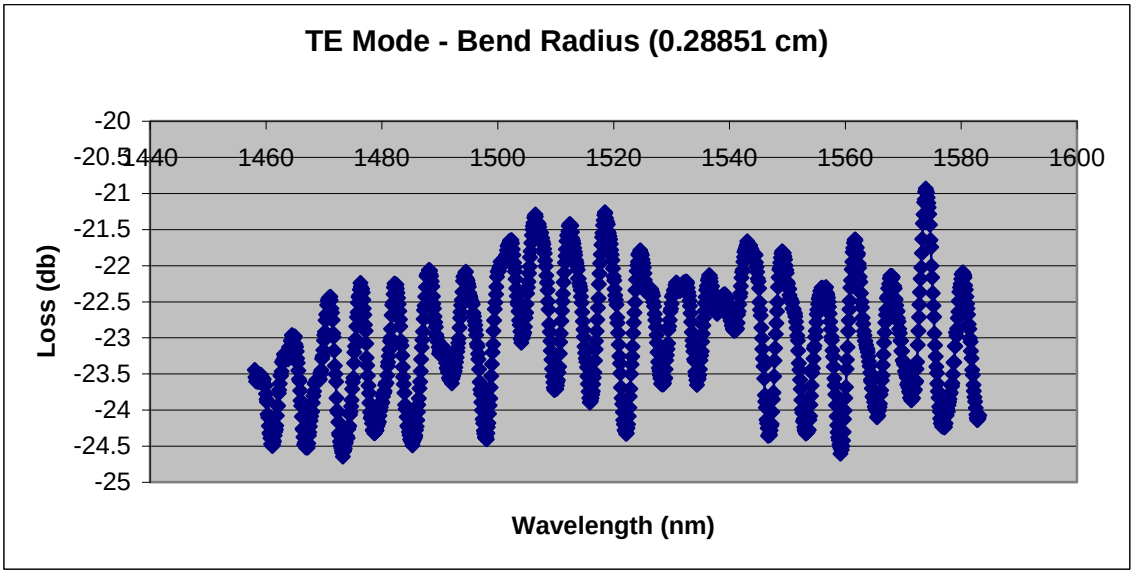
TE Mode - Bend Radius (0.28851 cm)
-20
-20.5
-21
-21.5
-22
-22.5
-23
-23.5
-24
-24.5
-25
Loss (db)
1440
1460
1480
1500
1520
1540
1560
1580
1600
Wavelength (nm)

(c)

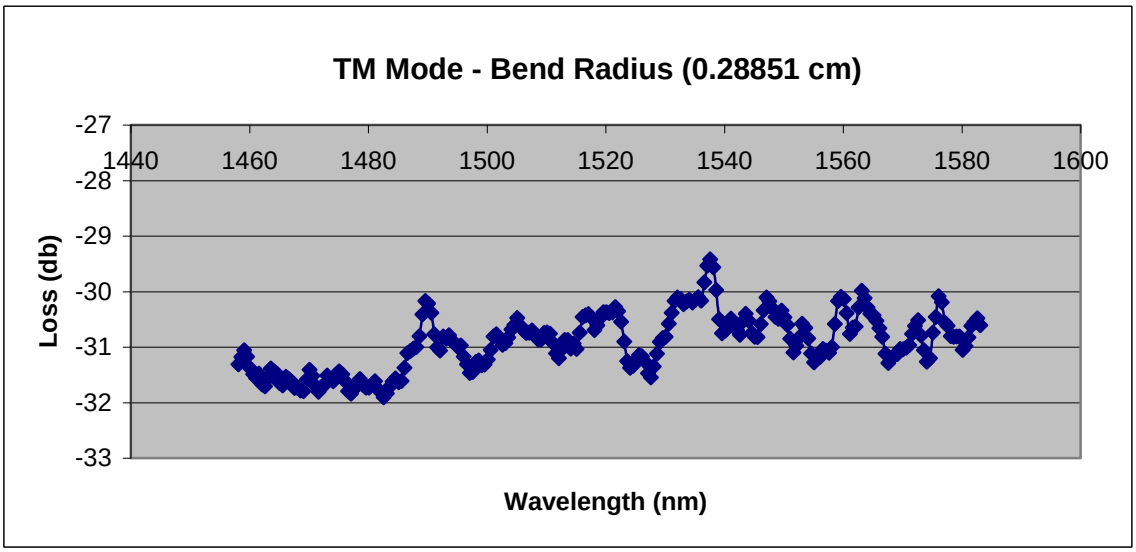

(d)

Figure 20 : Fabry Perot Interference (a) TE Mode without waveguide chip (b) TM Mode without waveguide chip (c) TE Mode with waveguide bend radius = 0.28851 cm (d) TM Mode with waveguide bend radius = 0.28851 cm

The Fabry-Perot interferences are caused by surfaces which reflect the light back and forth and that is why we see the oscillations. It is possible to determine the spacing of the surfaces causing these reflections by the period of oscillations. Since the oscillations occur even without the chip in place it can be concluded that the surfaces are in the optical set up. The cavity can be found using the formula:

$$\Delta\lambda_0 = \lambda_0^2 / 2*n*d$$

Where $\Delta\lambda_0$ the frere spectral wavelength, n is is the refractive index and d is the size of the cavity.

d = 240 μm in Air

= 160 μm in Glass

= 70 μm in Silicon

CHAPTER 3: EXPERIMENTAL LOSS MEASUREMENT

Experiments were conducted on a number of waveguides which were of the same total length with different bend radii. The dimensions of the waveguides experimented on are shown in Table 2. The light from the laser source was coupled to the waveguides through a lens. The output light was measured using an IR detector. The difference between the measured power with and without the chip in place gave the total loss of the waveguides which included the bending, mode mismatch, coupling, reflection and propagation losses.

To characterize the loss better the experiment was conducted on 11 waveguides. Figure 21 Shows the AutoCAD waveguides design. The arrow indicates the waveguides on which the experiment was conducted.

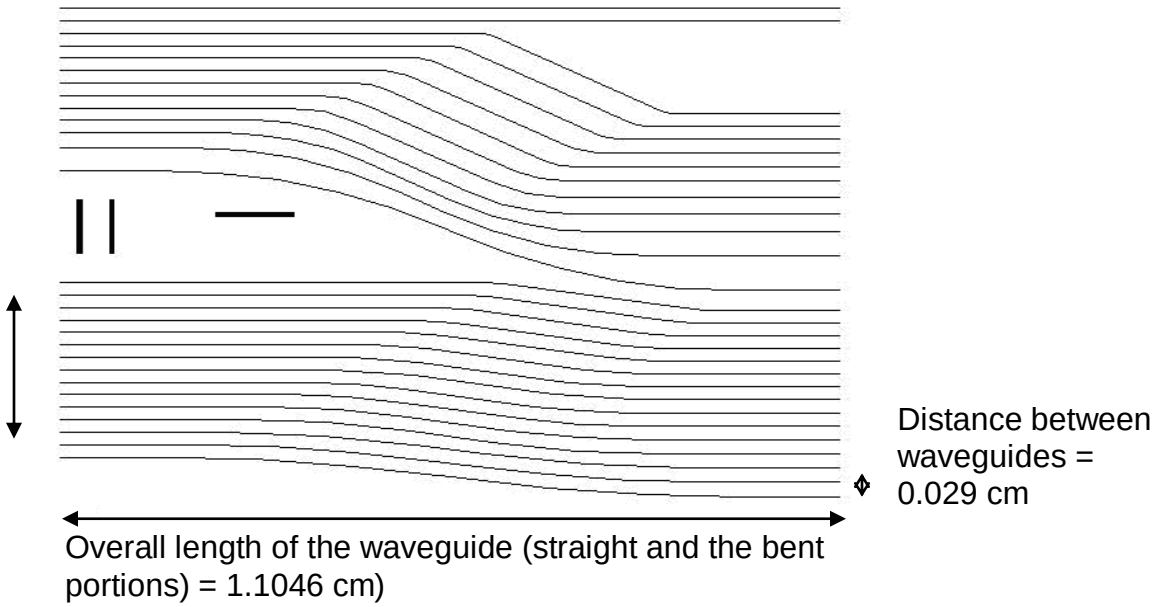

Figure 21 : Waveguide Design

Table 2 : Waveguide Dimension in cm

Bend Radii (cm)	Angle (degrees)	Arc Length (cm)	Added Line (cm)	Edge (per side)
0.28851	10	1.104601	0.269248	0.367322
0.34652	10	1.104601	0.262491	0.360576
0.41620	10	1.104601	0.254376	0.352472
0.49988	10	1.104601	0.244629	0.342740
0.60039	10	1.104601	0.232922	0.331052
0.72111	10	1.104601	0.218862	0.317012
0.86610	10	1.104601	0.201974	0.300150
1.04025	10	1.104601	0.181690	0.279898
1.24941	10	1.104601	0.157329	0.255573
1.50062	10	1.104601	0.128069	0.226358
1.80235	10	1.104601	0.092926	0.191268

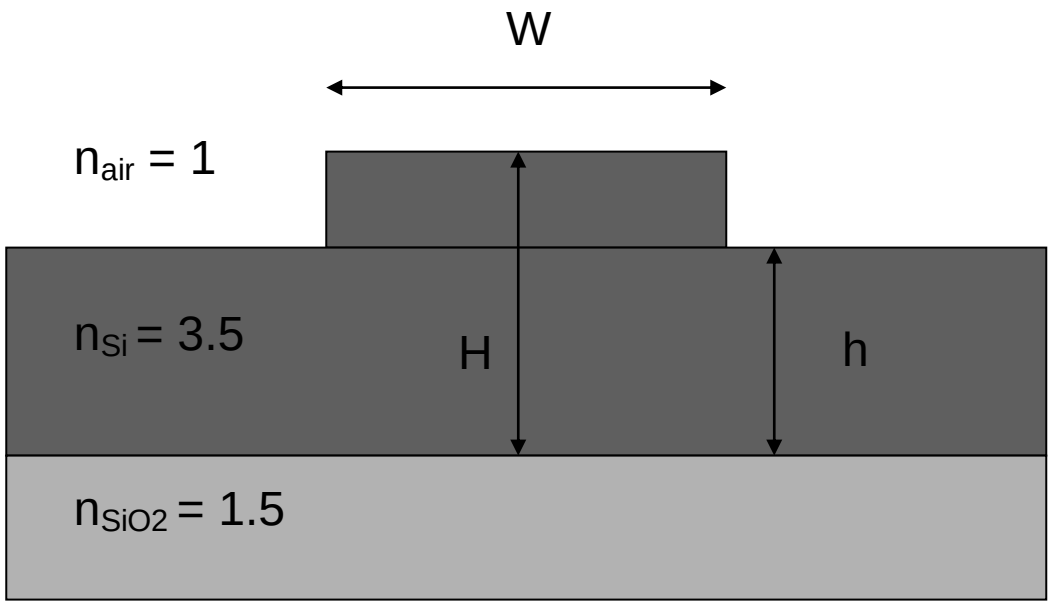

Figure 22 : Waveguide dimensions to calculate the single mode operation condition

The condition for a waveguide to support just one mode has been previously studied [16] and could be found using the equation below. Figure 22 explains the variables used in the equation.

$$W / H < \alpha + (r / \text{sqrt}(1 - r^2))$$

$$W / H = 5\mu / 3\mu = 1.67$$

$$\alpha = 0.3$$

$$r = h / H = 2.25\mu / 3\mu = 0.75$$

Right hand side of the equation is 1.67 and left hand side of the equation is 1.43 which does not satisfy the condition for single mode operation.

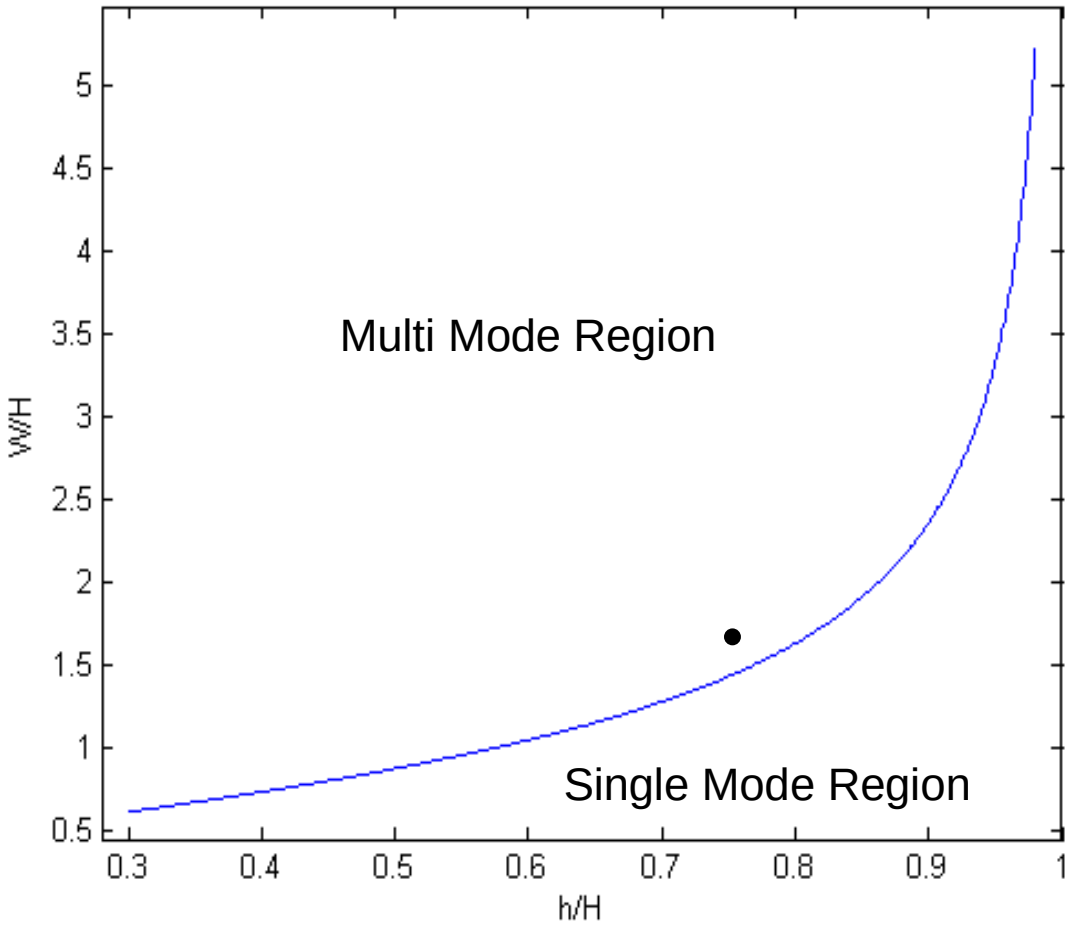

Figure 23 : Graph to indicate if the waveguide works in the single mode or multimode region

Figure 23 shows the line which separates the single mode and the multi mode region. The black dot represents the waveguide used for the experiments. It lies just on the boundary of the single mode and multi mode region.

3.1 OPTICAL CHIP DESIGN AND FABRICATION

The waveguides were each 1.1cm long with two identical curved sections of varying radii from 0.29 cm to 1.8 cm . The constant waveguide length allows bending loss to be distinguished from coupling, absorption, and scattering losses. In addition, the lateral offset between input and output waveguides minimizes the collection of unguided light in the sample.

The waveguides were fabricated on bonded and etched-back silicon-on-insulator wafers (Ultrasil Corporation) by Babitha Bommalakunta (University of Kentucky) and Mark Crain (University of Louisville). The buried oxide was 2μm thick and the bonded silicon epitaxial layer was 3μm thick. Waveguides were defined in positive photoresist using UV contact photolithography with image reversal. The waveguide pattern was etched 750nm deep into the silicon using a C2F8-SF6 process in an inductively coupled plasma system (STS PLC). The wafers were diced to expose the end facets which were subsequently polished using alumina polishing discs on a Beuhler Ecomet polishing system. Finally, we removed the photoresist with acetone and cleaned the die in a H_2O_2 and NH_4OH solution to remove any residue. Figure 24 shows SEM images of the fabricated waveguides.

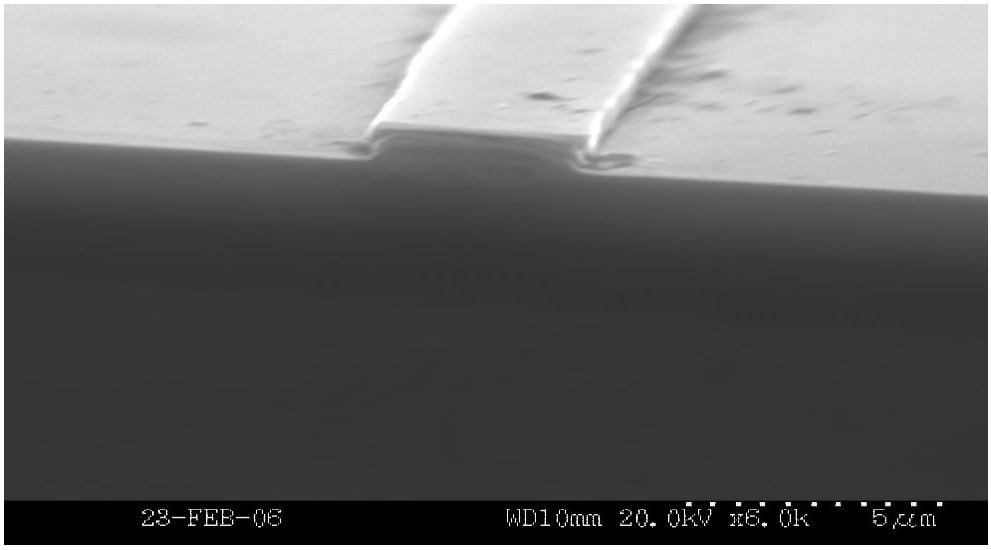

(a)

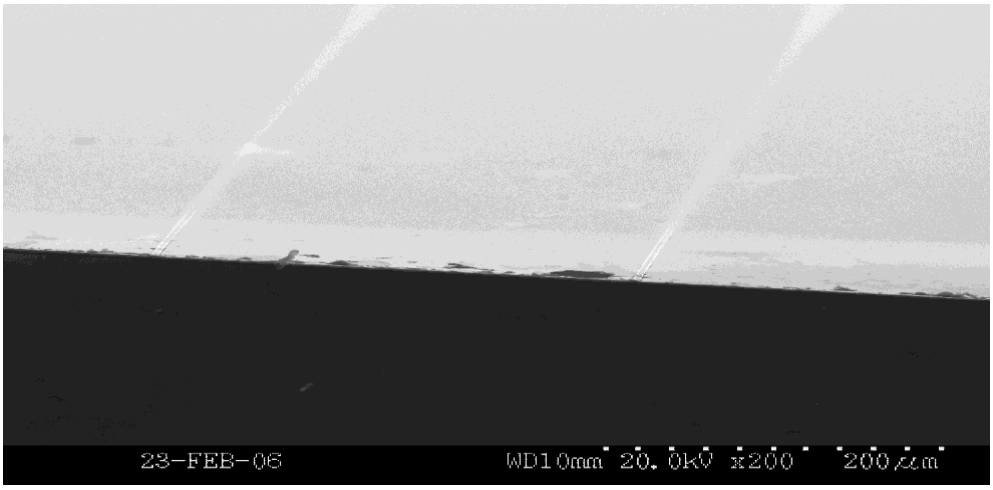

(b)

Figure 24 : Scanning Electron Microscopy image is the SOI waveguide (a) Closer view of a waveguide cross section (b) spacing between 2 waveguides

3.2 LOSS MEASUREMENTS

We performed loss measurements using a tunable laser source at 1550nm (Agilent 81680A) coupled to polarization maintaining optical fiber (OZ Optics Inc.). Light was coupled into the waveguide using a microscope objective (0.85 NA) and light was collected from the waveguide output using a second objective (0.4 NA). The aim of these experiments is to measure the relative power loss as the wave propagates through the waveguide. Therefore, even if the coupling efficiency from the lens to waveguide and from waveguide to lens is not very high, the relative coupling loss would still be a constant. This would merely shift the curve down by some amount which would represent the coupling loss and we would be able to isolate and analyze the bending loss Figure 25 shows the optical set up during the measurements. Figure 26 shows the waveguide chip. The lines that run across the chip are the waveguides. Figure 27 shows the light through the waveguide as imaged by the IR camera.

The input light was linearly polarized at approximately 45° to the waveguide axes. Fiber to waveguide alignment was performed using piezo driven flexure stages (Thorlabs MDT 616) and a near infrared camera (Hamamatsu C5332). An InGaAs detector (Agilent 81624A) was used for power measurements and a Glan-Taylor polarizer, AR coated for 1550nm wavelength, was used to select the TE or TM mode. Insertion loss was determined from the difference in transmitted power with and without the chip in place. Figure 28 shows the block diagram of the experimental setup indicating the various components used.

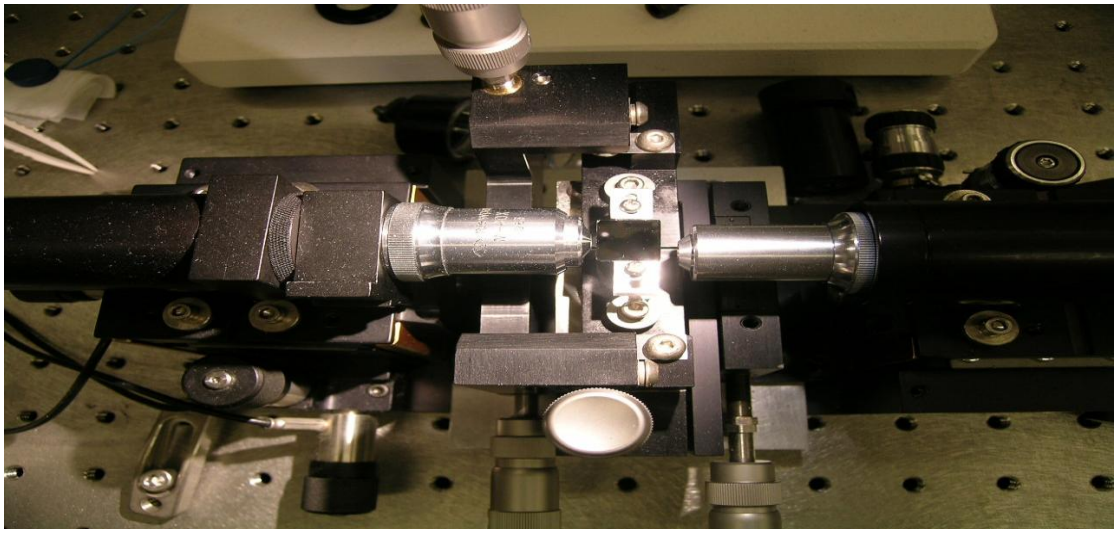

Figure 25 : Optical set up

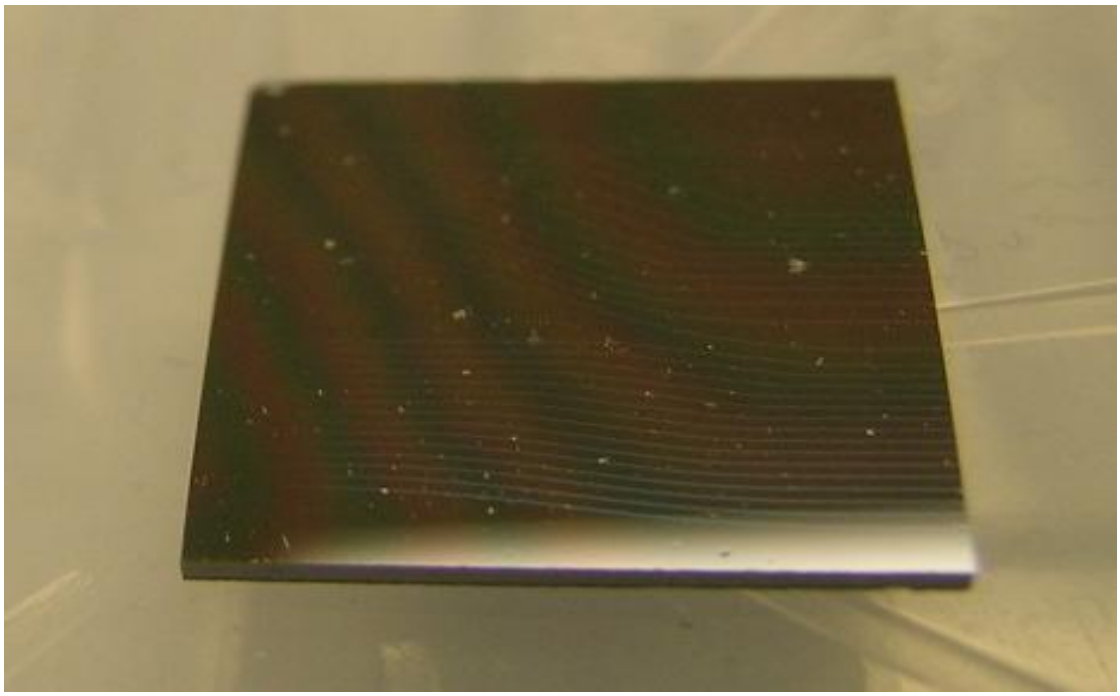

Figure 26 : Waveguide Chip

Figure 27 : Light through the waveguide as imaged on the IR camera.

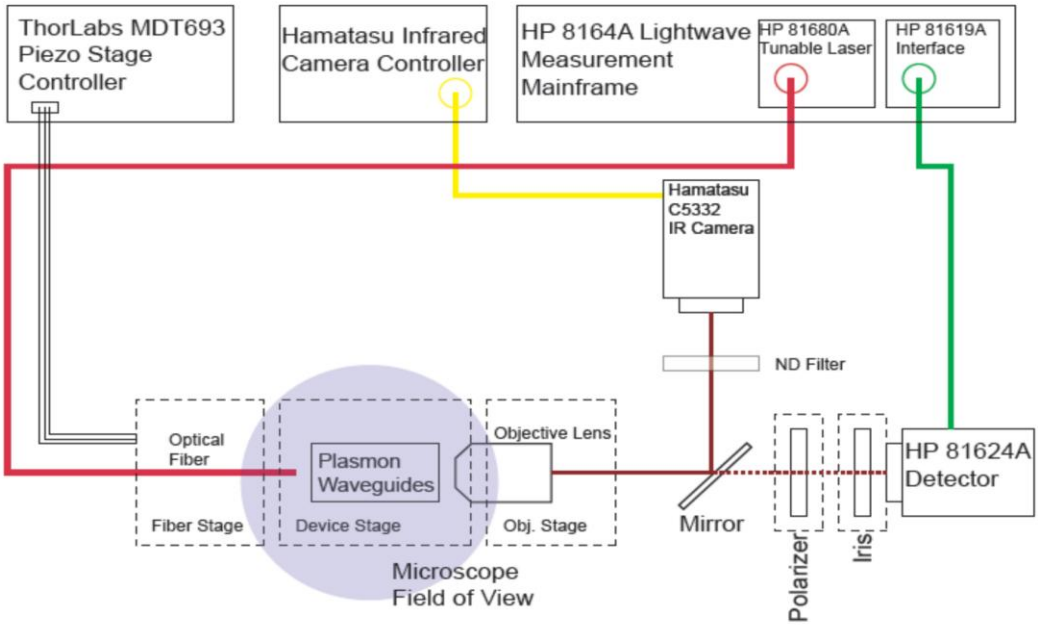

Figure 28 : Block Diagram of the Experimental set up

CHAPTER 4: COMPARISON OF SIMULATED AND EXPERIMENTAL LOSS

The experimental and simulated values of the loss for the TE and TM modes are shown in Figure 29. The difference in the experimental and the simulated measurements are attributed to absorption, and scattering losses. Since the waveguides are of identical cross section and equal lengths, these losses shift the experimental curves by constant value for all bend radii. The reflection loss was assumed to be 30% at each interface of the waveguide.

As expected, bend loss changes by a very small amount for large values of bend radius and starts to drastically increase as the bend radius becomes small which is approximately 0.8661 cm. This trend can be seen in the simulated and experimental values for both the TE and the TM modes. After accounting for scattering, absorption, and coupling losses, the experimental loss measurements agree well with the results of finite element analysis for an equivalent straight waveguide. For the TE mode this model follows the experimental trend with an almost constant offset of -11 dB and accurately predicts the radius at which the loss begins increasing rapidly.

For the TM modes, the equivalent straight waveguide model underestimates the increase in bend loss with decreasing radius slightly, but again helps predict a minimum radius for low loss design. The experimental bend loss in TE data at bend radius of 0.72111 cm, 1.50062 cm and 1.80235 cm are probably due to defects or could be caused by Fabry-Perot interference.

In both the TE and the TM modes the difference in the bending and the mode mismatch loss was found to be minimal for waveguides with large bend radius. For the waveguide with small bend radius the bending loss is found to be higher than the mode mismatch loss in the TE mode and the mode mismatch loss is higher than the bending loss in the TM mode. The bending and mode mismatch losses was found to be insignificant for waveguides with bend radii larger than approximately 1 cm and with the increase in the bending radius theses losses also increased and cannot be neglected.

If the coupling and reflection losses are added to the simulated values the difference in the TE and the TM mode is almost a constant for waveguides with high bend radius. But, for the waveguides with small bend radius there is a small difference in

the experimental and simulated values which could be attributed to the absorption in the bent portion as the scattering loss was found to be almost a constant.

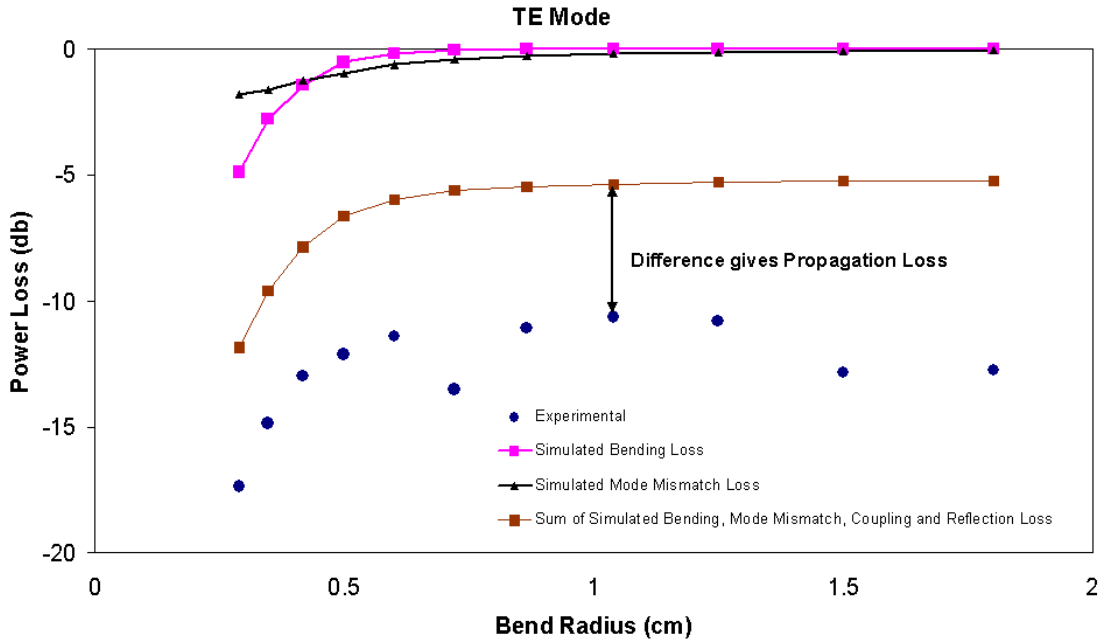

(a)

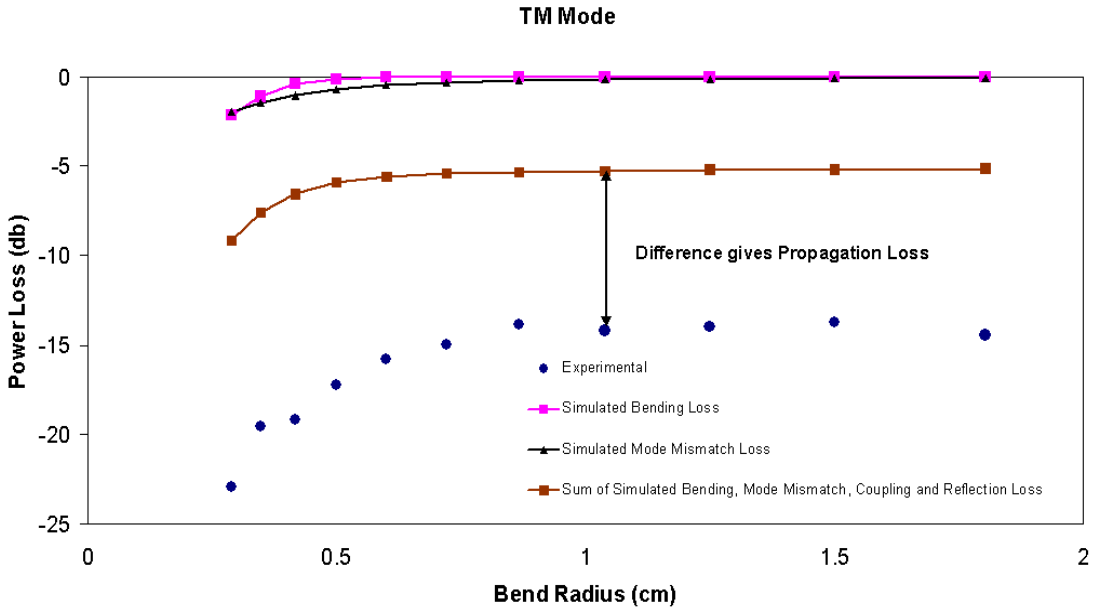

(b)

Figure 29 : Comparison of experimental and simulation loss data (a) TE mode (b) TM mode

CHAPTER 5: CONCLUSIONS AND FUTURE WORK

Good agreement between simulated and experimentally measured losses gives us confidence that bending loss can be accurately modeled in high-index contrast, large mode area waveguides using conformal mapping and finite element analysis with PML boundary conditions. Care must be taken in choosing the width and absorption coefficient for the PML regions, but a large range of values yield consistent results. Waveguide to waveguide variations in coupling efficiency, absorption, and scattering loss proved consistent enough to compare trends and minimum radii for low loss operation. However, these variables were not consistent enough in the present experiment to confidently quantify the simulation error. These results also reemphasize the inherent tradeoff between integration density and mode confinement and confirm that SOI rib waveguides behave more like low index contrast structures with regard to bending loss.

Silicon on Insulator waveguides are a significant part of dense integrated circuits and this thesis just analyses one particular type of waveguide. Waveguides could be fabricated with different dimensions, materials and design. As this thesis proves that finite element analysis is an accurate way to model waveguides, this method could be used to design waveguides which offer low bending loss.

REFERENCES

[1] B. Jalali and S. Fathpou, "Silicon Photonics," *Journal Of Lightwave Technology,* vol. 24, pp. 4600-4615, 2006.

[2] J. T. Hastings, M. H. Lim, J. G. Goodberlet, and H. I. Smith, "Optical waveguides with apodized sidewall gratings via spatial-phase-locked electron-beam lithography," *Journal of Vacuum Science & Technology B,* vol. 20, pp. 2753-2757, 2002.

[3] D. Dai and S. He, "Analysis of characteristics of bent rib waveguides," *Journal of the Optical Society of America A,* vol. 21, pp. 113-121, 2004.

[4] A. Nesterov and U. Troppenz, "A plane-wave boundary method for analysis of bent optical waveguides," *Journal of Lightwave Technology,* vol. 21, pp. 2434-2437, 2003.

[5] M. Heiblum and J. H. Harris, "Analysis of Curved Optical-Waveguides by Conformal Transformation," *IEEE Journal of Quantum Electronics,* vol. 1, pp. 75-83, 1975.

[6] V. Subramaniam, G. N. DeBrabander, D. H. Naghski, and J. T. Boyd, "Measurement of mode field profiles and bending and transition losses in curved optical channel waveguides," *Journal of Lightwave Technology,* vol. 15, pp. 990-997, 1997.

[7] W. W. Lui, C. L. Xu, T. Hirono, K. Yokoyama, and W. P. Huang, "Full-vectorial wave propagation in semiconductor optical bending waveguides and equivalent straight waveguide approximations," *Journal of Lightwave Technology,* vol. 16, pp. 910-914, 1998.

[8] W. Berglund and A. Gopinath, "WKB Analysis of Bend Losses in OpticalWaveguides," *Journal of Lightwave Technology,* vol. 18, pp. 1161-1166, 2000.

[9] H. Deng, G. H. Jin, J. Harari, J. P. Vilcot, and D. Decoster, "Investigation of 3-D Semivectorial Finite-Difference Beam Propagation Method for Bent Waveguides," *Journal of Lightwave Technology,* vol. 16, pp. 915-922, 1998.

[10] Y. Tsuji and M. Koshiba, "Complex modal analysis of curved optical waveguides using a full-vectorical finite element method with perfectly matched layer boundary conditions," *Electromagnetics,* vol. 24, pp. 39-48, 2004.

[11] P. Bienstman, E. Six, M. Roelens, M. Vanwolleghem, and R. Baets, "Calculation of bending losses in dielectric waveguides using eigenmode expansion and perfectly matched layers," *Ieee Photonics Technology Letters,* vol. 14, pp. 164-166, Feb 2002.

[12] J.-P. Berenger, "A Perfectly Matched Layer for the Absorption of Electromagnetic Waves," *Journal of Computational Physics,* vol. 114, pp. 185-200, 1994.

[13] K. Kakihara, N. Kono, K. Saitoh, and M. Koshiba, "Full-vectorial finite element method in a cylindrical coordinate system for loss analysis of photonic wire bends," *Optics Express,* vol. 14, pp. 1128-11141, 2006.

[14] T. E. Murphy, "Integrated Optical Grating-Based Matched Filters for Fiber-Optic Communications," in *Department of Electrical Engineering and Computer Science*: Massachusetts Institute of Technology, 1996.

[15] D. Marcuse, "Mode Conversion Caused by Surface Imperfections of a Dielectric Slab Waveguide," *Bell System Technical Journal,* vol. 48, pp. 3187-3215, Dec 1969.

[16] S. P. Pogossian, L. Vescan, and A. Vonsovici, "The Single-Mode Condition for Semiconductor Rib Waveguides with Large Cross Section," *Journal of Lightwave Technology,* vol. 16, pp. 1851-1853, 1998.

VITA

The author was born in Chennai, Tamil Nadu, India on December 9, 1983. In 2005, he completed is under graduation in India at Anna University, in the Department of Electrical and Electronics Engineering. In August 2005 he joined the University Of Kentucky to pursue his MS in Electrical Engineering. He was awarded Kentucky Graduate Scholarship and University of Kentucky tuition scholarship for his academic excellence. During the course of the program, he worked in the Department of Electrical Engineering as a Research Assistant